Journal of Applied Polymer Science

A Study of Graphene Oxide-Reinforced Rubber Nanocomposite

Bismark Mensah,[1] Sungjin Kim,[1] Sivaram Arepalli,[2] Changwoon Nah[1]

[1]BK21 Plus Haptic Polymer Composite Research Team, Department of Polymer-Nanoscience and Technology, Chonbuk National University, 567 Baekje-Daero, Jeonju 561-781, South Korea

[2]Education and Outreach, National Institute of Aerospace, 100 Exploration Way, Hampton, VA 23666-6701

Correspondence to: C. Nah (E-mail: cnah@jbnu.ac.kr)

ABSTRACT: Graphene oxide-reinforced acrylonitrile–butadiene rubber nanocomposites were prepared via solution mixing. The morphology of the graphene oxide was studied, and its successful dispersion within the rubber matrix was confirmed by transmission electron microscopy, scanning electron microscopy, and X-ray diffraction studies. The strong rubber-to-filler interaction was confirmed by swelling and mechanical reinforcing behaviors and thermal stability. Dielectric spectroscopy test indicated a marked improvement of about five times in the real part of permittivity. The electrical conductivity level was close to that of nonconductive materials. © 2014 Wiley Periodicals, Inc. J. Appl. Polym. Sci. **2014**, *131*, 40640.

KEYWORDS: elastomers; graphene and fullerenes; nanotubes; rubber

Received 29 November 2013; accepted 21 February 2014
DOI: 10.1002/app.40640

INTRODUCTION

Over the years, polymer nanocomposites have received significant attraction both in the industry and in the academia. This new class of multiphase materials contains dispersion of an ultrafine phase, typically in the range of 1 ~ 100 nm.[1,2] The ultrafine phase (usually, nanoparticles) improves the performance of these polymers by simply transferring their inherent properties such as strength, electrical, and other desired properties to the polymer materials. Elastomers, a category of polymers, have gain importance in the rubber industry for packaging, electro-optics, thermal, and other applications. They are usually reinforced with mineral fillers to obtain substantial improvements in strength and stiffness as well as other properties. The physical performance of the elastomeric material strongly depends on various parameters, including volume fraction, shape and size of particles, as well as filler–filler and filler–matrix interactions. The interaction between the filler particles and the rubber matrix is considered to be the most important aspect of the design.[3–6] The fabrication of elastomers would yield resilient products having gummy properties with limited strength without the inclusion of fillers.

The discovery of graphene[7] and the subsequent development of graphene-based polymer nanocomposites is an important addition in the field of nanoscale science and technology. The recent extensive interest in it is due to its excellent properties such as high thermal conductivity, high Young's modulus, large specific surface area, electromagnetic interference shielding, and electrical conductivity. These outstanding properties of graphene are utilized in various applications such as solar cells, field effect devices, practical sensors, and transparent electrodes.[8–10] Graphene has proven to be a multifunctional nanomaterial and is entering a crucial segment in its product lifecycle from innovation to applications. Opportunities for the future will depend on the effective use of graphene defects to design graphene polymer nanocomposites.[11] In recent years, studies have shown that the nanocomposites exhibited excellent electrical, mechanical, and thermal stability properties.[12–14]

Even though progress has been made in the use of graphene sheets as modifiers of polymer matrices, one main factor that limits the application of graphene is the poor compatibility between the pristine graphene sheets and the polymer matrix. In contrast to pristine graphene, there are plenty of oxygen-containing groups on the graphene oxide (GO) surface. These functional groups not only allow the good dispersion of GO in aqueous solution, but also facilitate the interaction between the host polymer and GO via covalent or noncovalent bonds.[15] It is therefore highly necessary to prepare GO/polymer nanocomposites carefully and study their novel properties. By taking the advantages of GO, several polymer matrices including thermosets, thermoplastics, and elastomers have been studied with noticeable improved property obtained by different mixing techniques.[12,13]

The acrylonitrile–butadiene rubber (NBR) is one of the most attractive polymer matrices in the polymer composites and is

Table I. Composition of GO/NBR Nanocomposites (in phr)

Ingredients	NBR	GO-NBR1	GO-NBR2	GO-NBR3	GO-NBR4
NBR	100	100	100	100	100
Sulfur	2	2	2	2	2
Zinc oxide	5	5	5	5	5
CZ	0.5	0.5	0.5	0.5	0.5
Stearic acid	1.5	1.5	1.5	1.5	1.5
TMTD	0.25	0.25	0.25	0.25	0.25
GO	0	0.1	0.5	1	2

phr, parts per hundred of rubber; CZ, *N*-cyclohexyl-2-benzothiazolysulfenamide; TMTD, tetramethylthiuram disulfide.

the workhorse of the industrial and automotive rubber products industry. By selecting an elastomer with the appropriate acrylonitrile content in balance with other properties, the rubber compounder can use NBR in a wide variety of application areas such as seals and hoses for fuel and oil.[16] Thus, the area of graphene–NBR composite requires critical attention focusing on the choice of graphene nanofiller, matrix, processing, and characterization techniques.

The current work is primarily centered on the study of preparation and properties of GO/NBR nanocomposite. Nonfunctionalized GO is directly added to NBR matrix via solvent mixing and then made into sheets using a roll-mill after complete evaporation of the solvent from the compound to achieve the desired level of reinforcement. Results of this comprehensive study are provided in the following sections, mainly characterizing the structural features, cure behavior, mechanical properties, thermal behavior, electrical property, and other physical properties of the prepared nanocomposites.

EXPERIMENTAL

Materials and Sample Preparation

NBR supplied by Kumho Petrochemical Co., Korea, under the trade name KNB 25LM was the polymer matrix used in this study. GO modified by Hummer's method (purity: 99 wt % and thickness: 0.7 ∼ 1.2 nm) was purchased from ENanotec Co., Korea. The compound formulation and the vulcanizing additives (zinc oxide, stearic acid, *N*-cyclohexyl-2-benzothiazolysulfenamide, tetramethylthiuram disulfide, and sulfur) are listed in Table I, expressed as parts per hundred parts of rubber (phr).

The preparation of the GO/NBR nanocomposite was successfully achieved via solution mixing method. The initial step involved the dissolution/dispersion of the as-received GO sheets in a solvent (dimethylfuran) by ultrasonication for about 2.5 h to disentangle the sheets that typically tend to cling together and form lumps, making it difficult to process. For this study, different GO solutions were prepared (varying GO by weight). Next step involved the dissolution of the rubber in a suitable organic solvent (acetone). A specific amount of rubber, which was reduced into smaller sizes by cutting, was added to a certain quantity of organic solvent (400 mL of acetone). This mixture was stirred vigorously by magnetic stirrer at 60°C until the rubber dissolved completely in the solvent. The prepared solutions of GO/dimethylfuran and NBR/acetone were mixed under vigorous magnetic stirring at 60°C for 12 h until a homogenous phase was observed. De-ionized water was gradually added to this mixture while stirring with a spatula to avoid sudden phase separation. This resulted in coagulation formation of the GO/NBR nanocomposite from the water phase (Figure 1). The resulting GO/NBR nanocomposite was oven dried at 80°C until the weight of the solid mass remained the same and free from trapped air.

The curing agents were added and mixed to obtain solid masses of GO/NBR nanocomposites in a two-roll mill (Farrel 8422, USA) and then were sheeted out. A cure rheometer analysis was carried on the samples to determine the optimum cure condition, which was used to cure the GO/NBR nanocomposites in a hot press (Caver WMV50H, USA) at a pressure of about 11 MPa and at 160°C with a mold of dimension 150 × 150 × 1 mm. The samples were cut into standard shapes and subjected to characterization analysis.

Characterization

X-ray Diffraction. X-ray diffraction (XRD) measurements (PANalytical X-PERT Powder diffractometer, the Netherlands) were carried out to characterize the structure of graphene, and the composites with Cu-Kα radiation (40 kV, 100 mA, $\lambda = 0.154$ nm). XRD patterns were obtained at room temperature based on continuous scan steps. The *d*-spacing of the particles was calculated using the Bragg's equation.

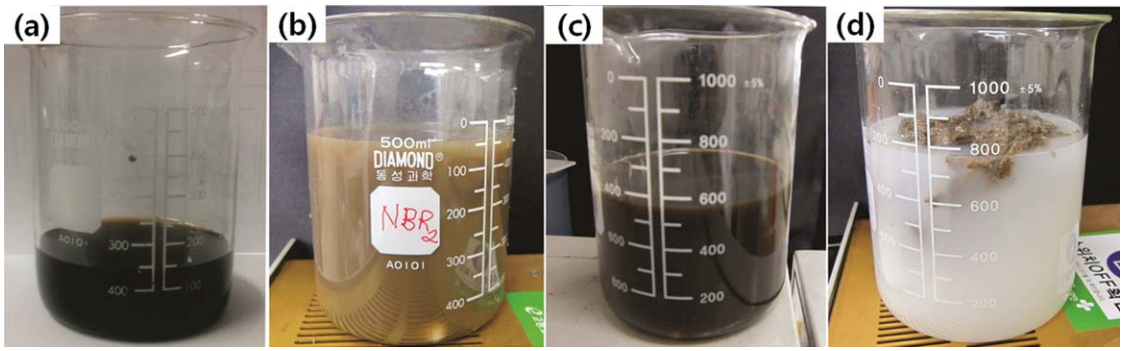

Figure 1. Photographs of solution mixing steps of the GO/NBR nanocomposites. (a) Exfoliated GO in dimethylfuran solution by ultrasonication; (b) GO-NBR2; (c) GO-NBR4 before coagulation; and (d) GO-NBR4 after coagulation. [Color figure can be viewed in the online issue, which is available at wileyonlinelibrary.com.]

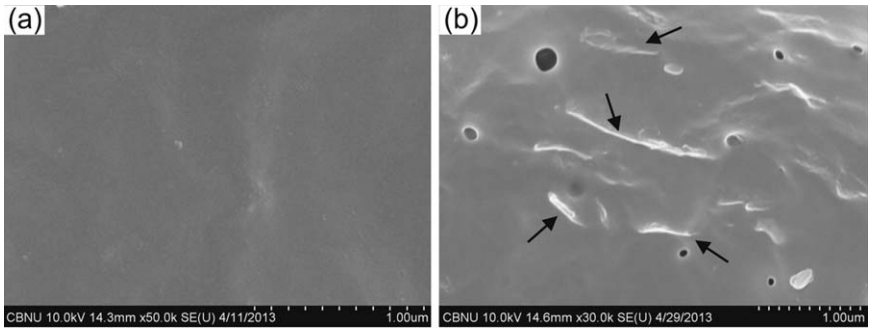

Figure 2. Field emission SEM images of 1 phr GO-filled rubber nanocomposites. (a) Unstrained and (b) after 20 min from a compression for 96 h.

Scanning Electron Microscopy. Cryogenic fracture surfaces of strained and unstrained specimens were coated by sputtering with platinum and then observed with field emission scanning electron microscope (JEOL, JSM 599, Japan).

Transmission Electron Microscopy. Ultrathin specimens (thinner than 100 nm) for transmission electron microscopy (TEM) observation were cryogenically cut with a diamond knife using an ultramicrotome (Leica Ultracut CUT, Germany) and collected on 200-mesh copper grids. The exfoliation of graphene nanosheets in NBR rubber was observed with transmission electron microscope (JEOL, JEM2100, Japan). The distribution of GOs within the NBR matrix was used to measure the efficacy of the solution mixing process of polymer nanocomposites.

Thermogravimetric Analysis. Thermogravimetric analysis (TGA) (TA Instrument, US/TA5000/TGA 2050) was used to investigate the thermal degradation behavior of the GO/NBR nanocomposite. The conditions were a nitrogen medium, equilibrium temperature of 25°C, and a heating rate of 10°C/min to a maximum temperature of 700°C.

Cross-Linking Density by Swelling Test. Swelling experiments of cured composites were performed by equilibrating them in toluene at room temperature for 48 h. The swelling degree Q_r was calculated using the relation[17];

$$Q_r = \frac{W_{sw} - W_i}{W_{dr}} \tag{1}$$

where W_i is the weight of the rubber sample before immersion into the solvent, W_{sw} and W_{dr} are the weights of the sample in the swollen state and after dried in an oven at 80°C for 2 h from its swollen state, respectively. The elastically active network chain density commonly referred as the cross-link density n, was calculated from Flory–Rehner equation[18];

$$-\ln(1-\upsilon_2) + \upsilon_2 + \chi_1 \upsilon_2^2 = V_1 n \left[\upsilon_2^{1/3} - \frac{\upsilon_2}{2}\right] \tag{2}$$

where υ_2 is the volume fraction of polymer in the swollen gel at equilibrium given by $(\frac{1}{Q_r})$, V_1 is the molar volume of the solvent (106.3 mL/mol for toluene), and χ_1 (0.35) is the polymer–solvent parameter determined from Bristow–Watson equation[19];

$$\chi_1 = \beta_1 + (\upsilon_s/RT)\left(\delta_s - \delta_p\right)^2 \tag{3}$$

where β_1 is the lattice constant, usually about 0.34, υ_s is the molar volume of solvent, R is the universal gas constant, T is the absolute temperature, δ is the solubility parameter, and the subscripts s and p refer to the swelling agent and polymer, respectively. The solubility parameters of NBR and the solvent toluene are 8.9 and 9.29 $(\text{cal/cc})^{1/2}$ respectively, according to the data taken from a polymer handbook.[20]

Electrical Resistivity. The surface resistance of the cured specimen cut into square shape (20 × 20 mm) with variable thickness was determined by a high-resistance meter (Keithley Electrometer 6517B) at room temperature. Careful measures were taken to ensure good contact of the specimen surface with the electrodes of the conduction tester. The distance between the conducting electrodes of the tester is about 5 mm. The resistance measured was converted to volume resistivity, ρ_v, using eq. (4)[21];

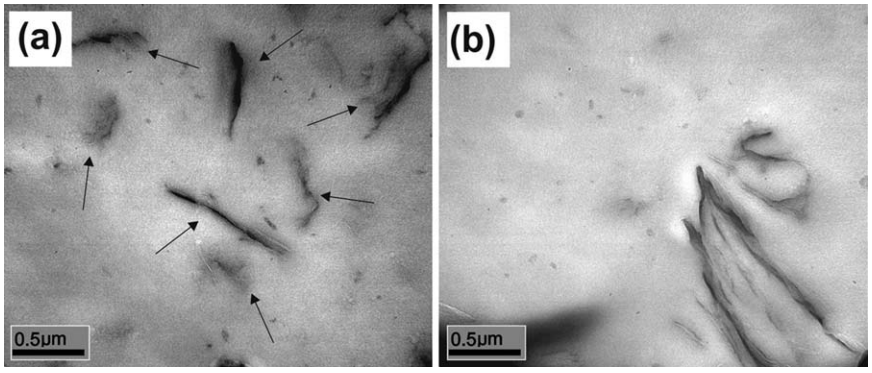

Figure 3. TEM images of 2 phr of GO-filled NBR nanocomposites. (a) Homogenous dispersion of GO in the NBR matrix. (b) Wrinkled GO sheets in the rubber matrix.

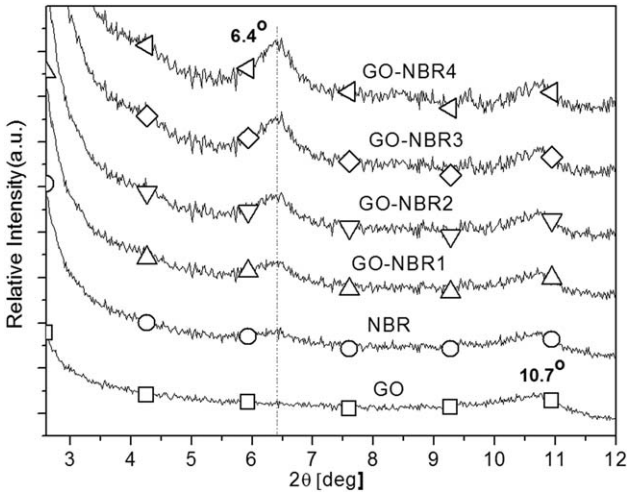

Figure 4. XRD patterns of GO and NBR loaded at different concentrations.

$$\rho_v = \frac{WTR}{L} \quad (4)$$

where W is the width, T is the thickness, L is the length of the sample, and R is the measured resistance. The reported values represented the mean of five samples each.

Dielectric Constant. The dielectric constant was measured by an LCR meter (VHR-200, USA). The frequency range selected was from 1 to 10^6 Hz, with steps of 1 Hz (for that was the optimum condition for the prepared samples). The top and bottom sides of the specimens were coated with conductive silver grease to improve the electrical contact between the specimens and the electrodes. The amount and number of silver coatings was maintained at the same rate to avoid variations in the thickness of the samples. The thickness of the samples is listed in Table IV. All measurements were carried at room temperature.

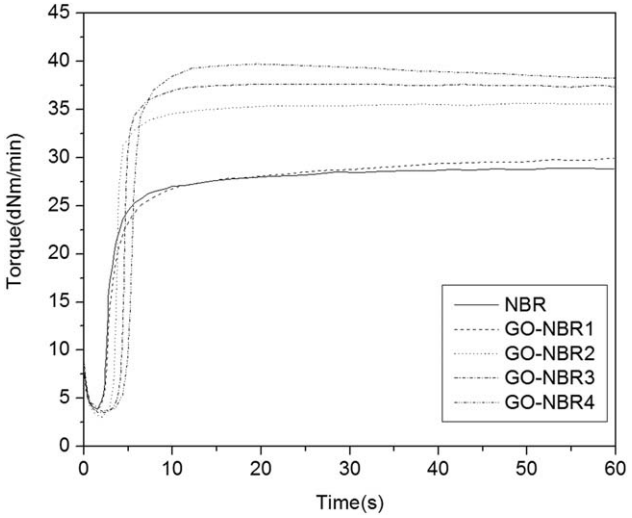

Figure 5. Cure behavior of GO filled with NBR compounds at 160°C hot press.

RESULTS AND DISCUSSION

Morphology and Dispersion of GO

Figure 2 shows the scanning electron microscopy (SEM) micrographs of the fractured surface of a representative sample loaded with 1 phr of GO. In the unstrained state, the sample appears smooth, and the dispersion of GO in the rubber matrix was not clearly observed. When the specimen was compressed via clamping for about 96 h, SEM observation after 20 min of straining shows protrusion of homogenously dispersed wrinkled sheets of GO out of the fractured surfaces.

This behavior is similar to our earlier study on carbon nanotube (CNT)-reinforced natural rubber nanocomposite[22]: when the specimen was stretched by about 15%, long coil-like CNTs with smooth surfaces were seen to protrude out of the fracture plane. When the strain was removed, the protruded CNTs slowly re-entered the rubber until only a few smooth outcrops of CNTs were observed after 15 min, and after 24 h the surface reverted back to the initial smooth condition. These observations gave direct evidence for weak interfacial interaction and easy slippage between CNTs and the rubber matrix.[22] In the current study of GO/NBR, it was observed that the GO sheets still maintained their degree of protrusion onto the rubber surfaces even after 20 min of release of the strain (compression). It can, therefore, be concluded that this is a possible indication of stronger interfacial interaction between the GO sheets and the rubber matrix. This was also confirmed by our TEM and XRD studies discussed later.

To further understand the dispersion of the nanoparticles within the rubber matrix, TEM analysis conducted [Figure 3(a)] illustrated a good dispersion of the GO sheets within the NBR matrix without any sign of agglomerates (indicated by arrows). Figure 3(b) shows the scrolling and folding effect of the edges of the GO sheets in the NBR matrix after compression. It has already been established that the corrugation and scrolling effect are part of the intrinsic nature of graphene nanosheets, which result from the fact that the 2D membrane structure becomes thermodynamically stable via bending.[23,24]

The homogenous distribution of GO in the NBR matrix was further confirmed by XRD analysis. As can be seen in Figure 4, the diffraction peak of GO appeared at $2\theta = 10.7°$ (corresponding d-spacing of about 0.92 nm), which is a typical peak of the layered GO, as noted earlier.[22] It can be seen from the curve that the peaks shifted to lower angles of around 6.4° (1.53 nm) after incorporation of the GO into the rubber matrix. This suggested an intense intercalation of the graphene sheets within the NBR matrix (Figure 4). Our studies, therefore, showed that solvent mixing is successful in the preparation of GO/NBR nanocomposites.

Cure Characteristics

The effect of GO on the cure properties of NBR nanocomposites was analyzed from the curing curves (Figure 5) at $T = 160°C$, and expressed in terms of scorch time, T_{S2}, optimum cure time, T_{90}, torque difference ($\Delta T = M_H - M_L$), and cure rate index (CRI) are reported in Table II. It can be seen that the scorch time (T_{S2}), which measures the incipient vulcanization of rubber, showed an increment after the addition of the

Table II. Curing Characteristics of NBR and GO/NBR Nanocomposites at $T = 160°C$

Compounds	M_H (dNm)	M_L (dNm)	$\Delta T(M_H - M_L)$ (dNm)	T_{90} (min)	T_{S2} (min)	Cure index $(100/T_{90} - T_{S2})$
NBR	29.4	3.75	25.7	10.50	2.30	12.2
GO-NBR1	29.5	3.80	26.1	14.30	2.37	8.4
GO-NBR2	35.5	3.40	32.1	5.48	3.11	42.42
GO-NBR3	37.6	3.50	34.1	6.16	3.86	43.5
GO-NBR4	39.7	3.73	36.0	7.58	4.50	32.5

nanofiller. According to Hernandez et al.[15] and Shanmugharaj et al.,[25] adding carbon-based fillers can delay the onset of vulcanization because of the presence of functional groups such as carboxylic acid and oxygen on the surface of the nanofillers that absorb the basic accelerator additives. Moreover, the unrestricted chain mobility among the NBR system at the start of curing could possibly be another reason for the retardation in the insipient vulcanization of the compounds. Generally, the delay of the premature vulcanization may be a desirable feature to increase the processing safety of the blend.[26] The optimum cure time was observed to be decreasing with increasing GO concentration, which demonstrated good dispersion of filler within the rubber matrix and could promote an increase in the rate of product formation. The CRI was also analyzed. Although there were some fluctuations in the experimental data, the CRI generally increased for GO-filled composites. This could be credited to the filler's ability to accelerate the vulcanization reaction. Furthermore, as cure occurs, reaction between GO and NBR might have occurred, and this introduced additional cross-links or network systems within the composite material. These networks, in turn, prevented chains from undergoing extended relative movement and, thus, contributed to the stiffness of the nanocomposites. This phenomenon may be responsible for the increase in the torque difference values ($\Delta T = M_H - M_L$) as the content of the GO increases (Table II). The improvement in the torque values is usually related to the degree of cross-linking, and hence its increase can be attributed to the increase in cross-linking density. The effect of an increase in cross-linking density also has a profound influence on the mechanical properties of the filled elastomers as discussed in the later part of this work.

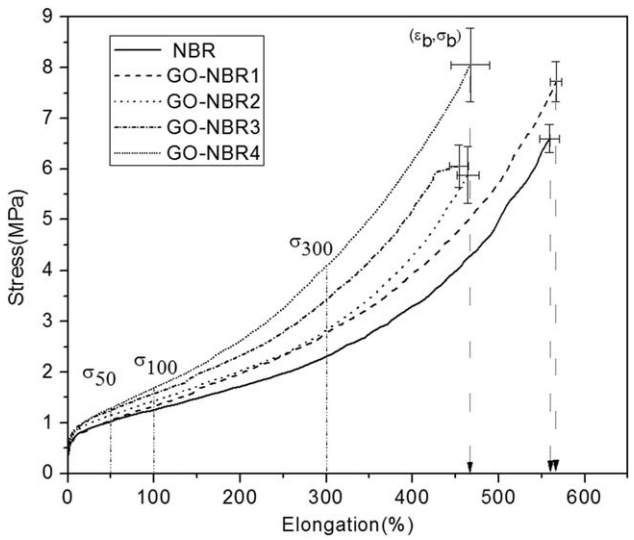

Figure 6. Stress–strain behavior of NBR nanocomposite at different concentrations of GO.

Tensile Property and Reinforcing Effect

The stress–strain curve of NBR filled with different amounts of GO nanofiller is presented in Figure 6, and their main properties are summarized in Table III. There was a considerable enhancement in the tensile properties with an increase in the GO concentration. All the tensile modulus parameters were exceptionally high for the GO-filled compounds except for the tensile strength (stress at break, δ_b). For instance, the compounds with filler content of 0.1 and 2 phr showed a rise in tensile strength up to 17% and 23%, respectively, at maximum stress level more than that of the neat rubber.

The improvement in the mechanical properties can be credited to better filler dispersion and good filler–rubber interaction. A good interfacial interaction between the GO sheets and the rubber is very essential for the nanocomposite to withstand load. Under load, the distributed load by the NBR matrix is carried predominantly by the GO nanofillers. In a recent study by Gudarzi and Sharif,[27] graphene layers enhanced the mechanical properties of the epoxy because of the strong interfacial adhesion and molecular level dispersion of the GO sheets through the epoxy matrix. However, the stress at break, δ_b, of the neat rubber was higher than that of the samples loaded with 1 and 0.5 phr GO concentration. This may be ascribed to internal and microscopic defects that were created during sample preparation and testing.

The elastic moduli of polymeric composites with the GO amount have been interpreted from the view of hydrodynamic effect. The values of elastic modulus at elongations of 50%, 100%, and 300%, respectively, were fitted to Einstein–Smallwood and Guth–Gold model[3,28] as shown in Figure 7. This is because they are the most applicable empirical equation for this kind of composite design. The equations are given by

$$\frac{E_f}{E_u} = 1 + 2.5\phi \tag{5}$$

$$\frac{E_f}{E_u} = 1 + 2.5\phi + 14.1\phi^2 \tag{6}$$

where, E_f and E_u are the moduli at a given elongation of filled and unfilled rubber, respectively, and ϕ is the volume fraction of GO fillers. Values of the relative elastic moduli obtained by

Table III. Tensile Properties of NBR and GO/NBR Nanocomposites

Tensile properties	NBR	GO-NBR1	GO-NBR2	GO-NBR3	GO-NBR4
Tensile strength (Mpa)	6.6 ± 0.28	7.7 ± 0.40	5.9 ± 0.56	5.9 ± 0.42	8.1 ± 0.73
50% modulus (Mpa)	1.03	1.05	1.15	1.25	1.30
100% modulus (Mpa)	1.27	1.34	1.44	1.58	1.70
300% modulus (Mpa)	2.31	2.77	2.83	3.43	4.08
Elongation at break (%)	559 ± 12	557 ± 7	464 ± 13	427 ± 11	467 ± 22

fitting the experimental data to eqs. (5) and (6) seemed to be much greater at lower volume fractions by comparison. This depicted extreme reinforcement attainment, which could be due to the effectiveness of the dispersion of GO sheets into the rubber matrix, strong interaction of filler-to-rubber, and the optimum curing level attained, which lead to the formation of resilient cross-links between the rubber and filler. Moreover, the nitrile groups of the NBR are well known to be good electron acceptors and, therefore, can interact more strongly with the electron-donating hydroxyl groups of the GOs.[29]

Alternatively, the reinforcement effect has also been confirmed by considering the changes in the rheological properties during vulcanization. In this case, the reinforcement parameter, α_f, has been calculated from the cure properties and compared with the volume fraction of the fillers. This was achieved by using the equation below[3,30]

$$\alpha_f = \frac{(M_\infty - M_i) - 1}{\left(M_\infty^0 - M_i^0\right) / \left(\frac{W_f}{W_r}\right)} \tag{7}$$

where M_i and M_∞ represent values for shear torques at start of vulcanization and the full cure for GO-filled rubber vulcanizates, respectively, M_i^0 and M_∞^0 are the corresponding values for the unfilled vulcanizates, and W_f and W_r represent the weights of GO and rubber, respectively. According to Donnet and Wolff groups,[31,32] the increase in shear torque for the filled compound can represent the contributions of rubber–filler interaction to the cross-linking process, if the filler is assumed not to affect the vulcanization mechanism of rubber. Figure 8 depicts the α_f for rubber vulcanizates filled with GO as function of the volume fraction of GO. The α_f increases by increasing the content of GO. Apparently, some fluctuations were obtained in the experimental data; higher values were generally observed for the rubber vulcanizates filled with GO nanofillers compared with the neat rubber. This is attributed to the increased interaction between the GO and the rubber. Nevertheless, the general tendency is that there is an enhancement of mechanical properties by GO fillers, which play the role of reinforcement, compared with the neat rubber.

Table IV. Electrical Volume Resistivity of NBR and GO/NBR Nanocomposites

Compounds	Thickness (mm)	Resistance (Ω)	Volume resistance (Ω cm)
NBR	1.25	2.59×10^{16}	3.27×10^{15}
GO-NBR1	1.24	3.02×10^{16}	3.74×10^{15}
GO-NBR4	1.19	3.66×10^{16}	4.36×10^{15}

Electrical Property

Table IV shows the effect of GO content on electrical volume resistivity of GO-reinforced NBR compounds. Large values of volume resistivity were obtained for all the GO-filled samples, and no discernable percolation threshold was observed even by increasing the volume fraction of the fillers. Interestingly, the current studies confirmed GO/NBR compounds as poor conductive materials with conductivity values around 10^{-15} S/cm. The lower conductivity is likely due to the blockage of ion movement by the GO network. The ions are either forced to take a more tortuous route or completely constrained by the GO network. This reduces the charge mobility, resulting in a reduction in the measured current.[33] However, electrical properties of nanocomposites depend primarily on the way the filler particles are distributed through the polymer matrix. At low levels of filler loading, the resistivity of the nanocomposite is slightly lower than that of the base polymer, because the filler particles begin to contact each other, and a continuous path is formed through the volume of the sample for electrons to travel. It was noted by researchers[29,34] that the material produced directly from GO is not particularly useful in view of conductor. A partial reduction of GO might be necessary to restore conductivity.[29]

Dielectric Property

Even though the measured electrical conductivity of the GO/NBR compound was very low, the compounds can also provide capacitive field grading from their increased dielectric constant. Figure 9 depicts the variation of the real part of dielectric permittivity (ε') and the loss factor with frequency. The GO-filled specimens attained significant improvement in the permittivity values at lower frequency compared with neat rubber. But this pattern decreased gradually at higher frequencies, whereas their respective loss factor reduced with increase in frequency.

The increment in the permittivity values for the compounds at lower frequency seemed to be plausible because at the low-frequency region, the alternation of the field is slow, thus providing sufficient time to permanent and induced dipoles to align themselves according to the applied field, leading to enhanced polarization. The enhanced values of (ε'), especially at low frequencies, can be attributed to increased conductivity, and/or interfacial polarization (IP), and/or electrode polarization. Other work suggests that the contribution of electrode

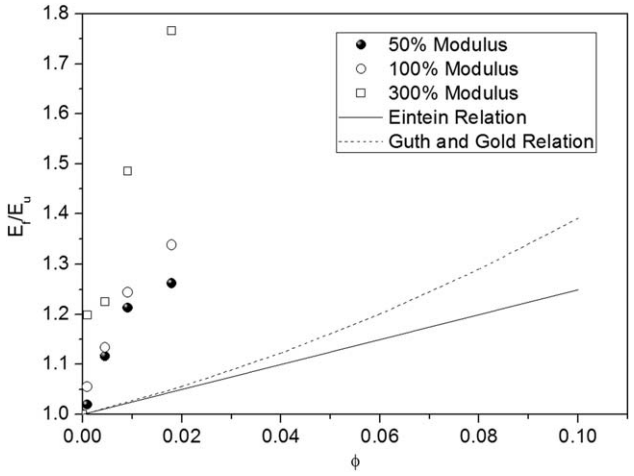

Figure 7. Reinforcement effect based on the change in modulus of GO/NBR nanocomposite.

polarization effects on the data can be very small, if care has been taken to ensure good ohmic contact between the electrodes and the sample, as in the case of the silver paint contacts.[35,36] Examined samples were tested under identical experimental conditions, having similar geometrical characteristics, and coated with conductive silver grease to enhance electrode contact. It can, therefore, be assumed that the electrode polarization contribution could have been the same for all the tested specimens. IP results from the accumulation of unbounded charges at the interfaces of the constituents, where they form large dipoles. Its intensity is connected to the extent of the existing interfacial area within the composite system, thus giving indirect evidence of the achieved distribution of nanoinclusions.[36] On this note, the higher values of ε' could be, to some degree, attributed to the enhanced conductivity and more significantly IP effect.

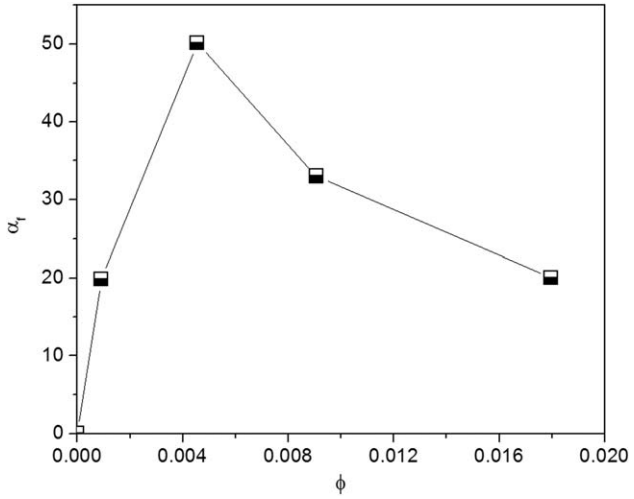

Figure 8. Reinforcement effect based on the change in rheological property during vulcanization as a function of volume fraction of rapheme oxide.

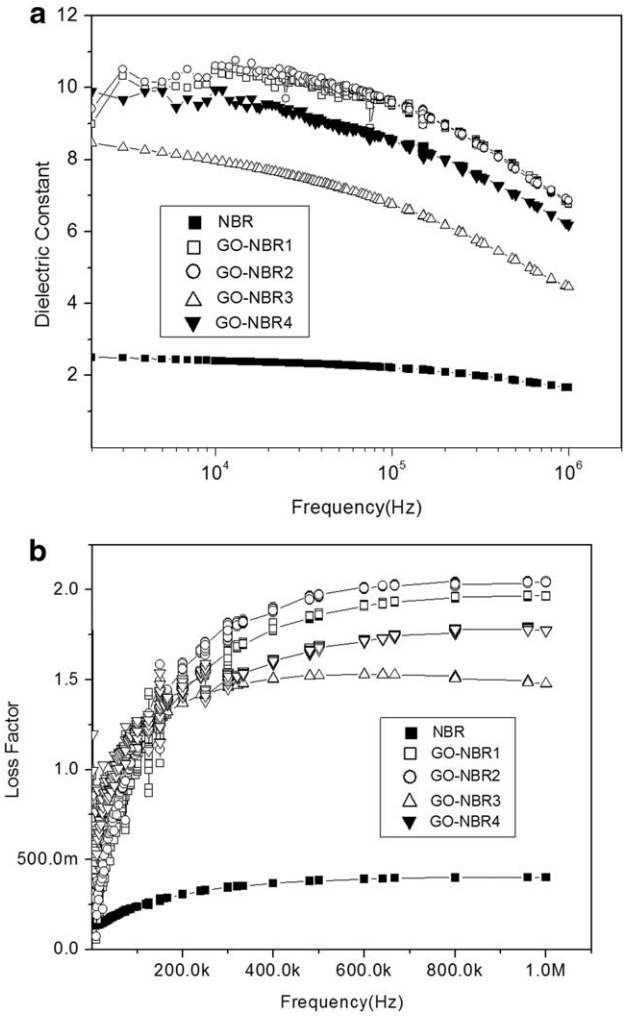

Figure 9. (a) Dielectric constant and (b) loss factor of GO/NBR nanocomposites at different filler concentrations.

Thermal Degradation

The thermal degradation behavior of NBR at different GO loadings is depicted in Figure 10 based on TGA. The temperature corresponding to the 5 wt % loss was taken as the initial

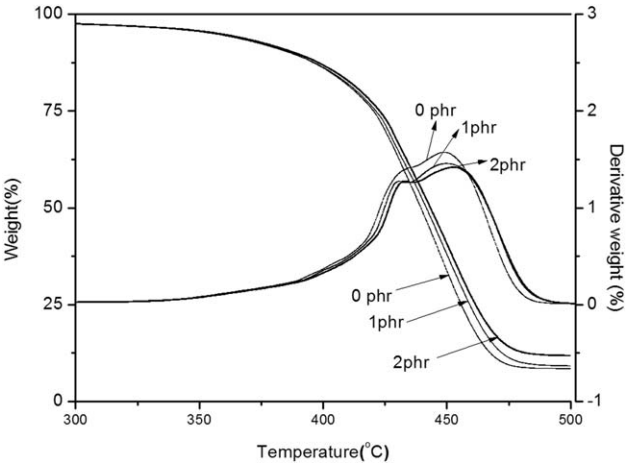

Figure 10. TGA and derivative thermogram of representative GO/NBR nanocomposites at different filler loadings of 0, 1, and 2 phr.

Table V. Equilibrium Swelling Ratio (Q_r), Their Relative Values (Q_r/Q_0) of GO-Filled to Unfilled NBR, and Cross-Linking Density (n)

Compounds	Q_r	Q_r/Q_0[a]	n (mol/cm^3)
NBR	2.68	1	7.87×10^{-4}
GO-NBR1	2.24	0.84	1.35×10^{-3}
GO-NBR2	2.12	0.79	1.53×10^{-3}
GO-NBR3	2.01	0.75	1.84×10^{-3}
GO-NBR4	1.91	0.71	2.06×10^{-3}

[a] Q_0 is the swelling ratio of the unfilled NBR.

degradation temperature (T_{onset}), and the temperature corresponding to the maximum value (peak) in derivative thermogram as the maximum degradation temperature (T_{max}). One distinct degradation peak pattern was observed; the T_{onset} slightly shifted to lower temperature, and T_{max} slightly shifted to higher temperature. Thermal degradation temperature was characterized by the maximum weight loss rate in TGA. Our result obtained indicated that the decomposition of the GO/NBR compound was somewhat lower than that of the neat rubber. For instance, GO/NBR4 recorded the least weight loss (88.4%) at 452°C (T_{max}), whereas the neat rubber recorded 92% at 447°C (T_{max}). This suggested a significant improvement in thermal stability of GO/NBR nanocomposites. The reason for the thermal enhancement could be attributed to restricted chain mobility of polymer near the graphene surface. During combustion, inflammable anisotropic nanoparticles can form a jammed network of char layers that retard transport of the decomposition products.[12,29] The enhanced thermal stability again supports the good dispersion of GO and strong interfacial interaction between GO and NBR.

Cross-Linking Density by Swelling

Table V shows the values of Q_r and Q_r/Q_0, where Q_0 is the swelling ratio for the unfilled NBR. The reduction in the equilibrium swelling ratio Q_r is a measure of the degree of total network by either rubber molecules or adhesion between the rubber chains and the filler particles.[36] A significant reduction in Q_r is seen in the GO/NBR compounds, notably GO-NBR1 and GO-NBR2, relative to the neat NBR. This might due to a strong interaction between the electron acceptor groups (acrylonitrile) in the NBR and the electron donating hydroxyl groups on the GO surfaces.[29] When the elastomer chains interact more strongly with the filler, a single macromolecular chain can cover sizable numbers of active sites on the filler surface, and therefore, only a smaller number of chains may be anchored at the surfaces.[28] The cross-linking densities n of GO-NBR compounds (Table V) increased significantly with increase in the filler volume fraction. This can be attributed to the effective filler-to-rubber links upon curing, leading to the reduction in the relative swelling ratio of GO-NBR compounds.[3] The increased network is responsible for the enhanced mechanical performance.

CONCLUSIONS

Successful dispersion of GO in the rubber matrix was confirmed by the changes in the interlayer distance calculated from the XRD data, and the homogenous distribution of nanoparticles in NBR matrix from the TEM and SEM images.

The cured samples attained excellent cure properties. For instance, the increment in the torque values (M_H, M_L, and ΔT) as a result of the GO concentration is a clear evidence for good reinforcement effect. Moreover, the GO surface rich of functional groups, defects, and other irregularities ensures a strong rubber-to-filler interaction. Such filler matrix interaction is the cause for improved properties such as resistance to solvent swelling, thermal stability, and improved mechanical properties of the GO/NBR compounds relative to that of the neat NBR rubber.

The electrical conductivities of representative samples showed virtually no improvement even with the increase in the filler volume fractions of the nanocomposite, whereas a noticeable enhancement of real part of dielectric constant was observed (about five times that of the neat rubber at a selected frequency of about 10 kHz).

ACKNOWLEDGMENTS

This work was supported by the research fund from Korea Institute of Energy Technology Evaluation and Planning (KETEP).

REFERENCES

1. Yuan, Q.; Misra, R. D. K. *Mater. Sci. Technol.* **2006**, *22*, 742.
2. Basuli, U.; Lee, G.-B.; Jang, S. Y.; Oh, J.; Lee, J. H.; Kim, S. C.; Jeon, N. D.; Huh, Y. I.; Nah, C. *Elast. Compos.* **2012**, *47*, 297.
3. Bokobza, L. *Macromol. Mater. Eng.* **2004**, *289*, 607.
4. Jang, S.-H.; Kim, W.-S.; Kang, Y.-G.; Han, M.-H.; Chang, S.-M. *Elast. Compos.* **2013**, *48*, 94.
5. Jang, S.-H.; Kim, W.-S.; Kang, Y.-G.; Han, M.-H.; Chang, S.-M. *Elast. Compos.* **2013**, *48*, 103.
6. Kim, D.-W.; Kim, C.-H.; Jung, H.-K.; Kang, Y.-G. *Elast. Compos.* **2013**, *48*, 114.
7. Novoselov, K. S. *Science* **2004**, *306*, 666.
8. Geim, A. K. *Science* **2009**, *324*, 1530.
9. Jang, B. Z.; Zhamu, A. *J. Mater. Sci.* **2008**, *43*, 5092.
10. Hwang, S. O.; Lee, B. H.; Cho, U. R. *Elast. Compos.* **2012**, *47*, 238.
11. Mukhopadhyay, P.; Gupta, R. K. *Plast. Eng.* **2011**, *67*, 32.
12. Wang, Y.; Shi, Z.; Fang, J.; Xu, H.; Yin, J. *Carbon* **2011**, *49*, 1199.
13. Kuilla, T.; Bhadra, S.; Yao, D.; Kim, N. H.; Bose, S.; Lee, J. H. *Prog. Polym. Sci.* **2010**, *35*, 1350.
14. Baia, X.; Wan, C.; Zhang, Y.; Zhaia, Y. *Carbon* **2011**, *49*, 1608.
15. Hernandez, M.; Bernal, M. d. M.; Verdejo, R.; Ezquerra, T. A.; López-Manchado, M. A. *Compos. Sci. Technol.* **2012**, *73*, 40.
16. Charrier, J.-M. Polymeric Materials and Processing; Hanser Publishers: New York, **1990**; p 202.

17. Le, H. H.; Hoang, X. T.; Das, A.; Gohs, U.; Stoeckelhuber, K.-W.; Boldt, R.; Heinrich, G.; Adhikari, R.; Radusch, H.-J. *Carbon* **2012**, *50*, 4543.
18. Flory, P. J. *J. Chem. Phys.* **1950**, *18*, 108.
19. Bristow, G. M.; Watson, W. F. *Trans. Faraday Soc.* **1958**, *54*, 1731.
20. Brandrup, J.; Immeraut, E. H. Polymer Handbook; Wiley :New York, **1974**; pp IV, 344–352.
21. Seo, M.-K.; Park, S.-J. *Chem. Phys. Lett.* **2004**, *395*, 44.
22. Nah, C.; Lim, J. Y.; Cho, B. H.; Hong, C. K.; Gent, A. N. *J. Appl. Polym. Sci.* **2010**, *118*, 1574.
23. Li, Y.; Wang, Q.; Wang, T.; Pan, G. *J. Mater. Sci.* **2011**, *47*, 730.
24. Shen, J.; Hu, Y.; Shi, M.; Lu, X.; Qin, C.; Li, C.; Ye, M. *Chem. Mater.* **2009**, *21*, 3518.
25. Shanmugharaj, A. M.; Bae, J. H.; Lee, K. Y.; Noh, W. H.; Lee, S. H.; Ryu, S. H. *Compos. Sci. Technol.* **2007**, *67*, 1813.
26. Sangwichien, C.; Sumanatrakool, P.; Patarapaiboolchai, O. *Chiang Mai J. Sci.* **2008**, *35*, 141.
27. Gudarzi, M.; Sharif, F. *Express Polym. Lett.* **2012**, *6*, 1017.
28. Perez, L. D.; Zuluaga, M. A.; Kyu, T.; Mark, J. E.; Lopez, B. L. *Polym. Eng. Sci.* **2009**, *49*, 872.
29. Kim, H.; Abdala, A. A.; Macosko, C. W. *Macromolecules* **2010**, *43*, 6515.
30. Nah, C.; Huh, M.-Y.; Rhee, J. M.; Yoon, T.-H. *Polym. Int.* **2002**, *51*, 510.
31. Ou, Y.-C.; Yu, Z.-Z.; Vidal, A.; Donnet, J. B. *Rubber Chem. Technol.* **1994**, *67*, 834.
32. Wolff, S. *Kautsch. Gummi Kunstst.* **2007**, *23*, 7.
33. Wang, Z.; Nelson, J. K.; Hillborg, H.; Zhao, S.; Schadler, L. S. *IEEE* **2012**, *19*, 40.
34. Young, R. J.; Kinloch, I. A.; Gong, L.; Novoselov, K. S. *Compos. Sci. Technol.* **2012**, *72*, 1459.
35. Tantis, I.; Psarras, G. C.; Tasis, D. *Express Polym. Lett.* **2012**, *6*, 283.
36. Tsangaris, G. M.; Psarras, G. C.; Kouloumbi, N. *J. Mater. Sci.* **1998**, *33*, 2036.